1 **Loss of E-cadherin enhances IGF1-IGF1R pathway activation and sensitizes breast**

2 **cancers to anti-IGF1R inhibitors**

3

4 Alison M. Nagle[1,2], Kevin M. Levine[1,3], Nilgun Tasdemir[1,2], Julie A. Scott[1,2], Kara Burlbaugh[2],

5 Justin Kehm[2], Tiffany A. Katz[1,2,4], David N. Boone[2,5], Britta M. Jacobsen[6], Jennifer M.

6 Atkinson[1,2], Steffi Oesterreich[1,2,3], Adrian V. Lee[1,2,7]

7

8 1. Dept. of Pharmacology and Chemical Biology, University of Pittsburgh, Pittsburgh, PA

9 2. Women's Cancer Research Center, UPMC Hillman Cancer Center, Magee Women's

10 Research Institute, Pittsburgh, PA

11 3. Dept. of Pathology, University of Pittsburgh, Pittsburgh, PA

12 4. The Center for Precision Environmental Health, Dept. of Molecular and Cellular Biology,

13 Baylor College of Medicine, Houston, TX (current)

14 5. Dept. of Biomedical Informatics, University of Pittsburgh, Pittsburgh, PA

15 6. Dept. of Pathology, University of Colorado Anschutz Medical Campus, Aurora, CO

16 7. Dept. of Human Genetics, University of Pittsburgh, Pittsburgh, PA

17

18 <u>Keywords</u>: breast cancer, invasive lobular carcinoma, insulin-like growth factor 1 receptor

19 (IGF1R), E-cadherin, growth factor signaling

20

25

26

27   Corresponding author:

28   Adrian V. Lee (leeav@upmc.edu)

29   Magee Women's Research Institute, A412

30   204 Craft Ave Pittsburgh, PA 15213

31   Phone: 412-641-7557; Fax: 412-641-2458

32

33   The authors declare no potential conflicts of interest.

34

35

36 **STATEMENT OF SIGNIFICANCE**

37 IGF1R signaling is an attractive therapeutic target in breast cancer due to its regulation of

38 proliferation, migration, and invasion. However, clinical trials targeting IGF1R have largely been

39 unsuccessful due to lack of biomarkers to stratify patients for therapeutic response. In this

40 study, we demonstrate loss of E-cadherin as a potential biomarker for response to anti-IGF1R

41 therapy, and show efficacy of IGF1R inhibition in ER+ ILC in combination with endocrine

42 therapy. Patients with ER+ ILC have poorer long-term outcomes than patients with ER+ IDC

43 and have a propensity for increased late recurrences, highlighting the need for improved

44 therapeutic strategies for this subtype of breast cancer. Here, we credential IGF1R inhibition as

45 a novel therapeutic strategy in combination with endocrine therapy for the treatment of ER+ ILC.

46

47

48

49

50

51

52

53

54

55

56

57

58

59

60

61

62   **ABSTRACT**

63   Purpose: Insulin-like growth factor I (IGF1) signaling regulates breast cancer initiation and

64   progression and associated cancer phenotypes. We previously identified E-cadherin (*CDH1*) as

65   a repressor of IGF1 signaling and in this study examined how loss of E-cadherin affects IGF1R

66   signaling and response to anti-IGF1R therapies in breast cancer.

67   Experimental Design: Breast cancer cell lines were used to assess how altered E-cadherin

68   levels regulate IGF1R signaling and response to two anti-IGF1R therapies. *In situ* proximity

69   ligation assay (PLA) was used to define interaction between IGF1R and E-cadherin. TCGA

70   RNA-seq and RPPA data was used to compare IGF1R activation in estrogen receptor positive

71   (ER+) invasive lobular carcinoma (ILC) and invasive ductal carcinoma (IDC) tumors. ER+ ILC

72   cell lines and xenograft tumor explant cultures were used to evaluate efficacy to IGF1R pathway

73   inhibition in combination with endocrine therapy.

74   Results: Diminished functional E-cadherin increased both activation of IGF1R signaling and

75   efficacy to anti-IGF1R therapies. PLA demonstrated a direct endogenous interaction between

76   IGF1R and E-cadherin at points of cell-cell contact. Increased expression of IGF1 ligand and

77   levels of IGF1R phosphorylation were observed in E-cadherin deficient ER+ ILC compared to

78   IDC tumors. IGF1R pathway inhibitors were effective in inhibiting growth in ER+ ILC cell lines

79   and synergized with endocrine therapy and similarly IGF1R inhibition reduced proliferation in

80   ILC tumor explant culture.

81   Conclusions: We provide evidence that loss of E-cadherin hyperactivates the IGF1R pathway

82   and increases sensitivity to IGF1R targeted therapy, thus identifying the IGF1R pathway as a

83   potential novel target in E-cadherin deficient breast cancers.

84

85

86

87 **INTRODUCTION**

88 IGF1 is a circulating endocrine hormone that is a major regulator of organismal growth and

89 development[1]. IGF1, in combination with estrogen, is essential for normal mammary gland

90 development, and this pathway is deregulated in the initiation and progression of breast

91 cancer[2–5]. Many studies, including from our laboratory, have shown the ability of the IGF1

92 receptor (IGF1R) to promote mammary tumorigenesis and metastasis[6–9]. Additionally, we

93 showed that when constitutively activated, IGF1R transformed mammary epithelial cells,

94 increased migration and invasion, and induced epithelial to mesenchymal transition (EMT) via

95 the NFkB pathway and upregulation of Snail[6,10].

96 Based on these observations, both small molecule tyrosine kinase inhibitors and monoclonal

97 antibodies against IGF1R were tested in clinical trials in breast cancer. Unfortunately, although

98 as many as 50% of breast tumors express IGF1R[11], these trials only identified a small subset of

99 patients showing a therapeutic response to IGF1R targeted therapy, suggesting that predictive

100 biomarkers are required to identify which patients' tumors will be responsive[12–15].

101 We previously developed an IGF1-signature (IGF-sig) based on microarray analyses, and more

102 recently reported a novel computational method to identify putative biomarkers of IGF1 signaling

103 using a systems biology approach[16]. The latter was based on a proteomic screen using reverse

104 phase protein array (RPPA) on 21 breast cancer cell lines stimulated with IGF1 over a time

105 course[17]. This computational model identified E-cadherin as a putative regulator of IGF1

106 signaling, and data in the present study indicate that loss of E-cadherin expression can directly

107 increase IGF1R pathway activation and associated phenotypes in breast cancer. Insight into

108 how E-cadherin regulates IGF1R is necessary to aid in our understanding of the oncogenic

109 signaling network, specifically because the loss of E-cadherin i) is implicated in the ability of

110 tumor cells to escape the primary tumor to potentially seed metastatic lesions and ii) is

111 transcriptionally repressed and/or genetically lost in subsets of breast tumors[18–22].

112   One such subtype of breast cancer with diminished E-cadherin expression is invasive lobular

113   breast carcinoma (ILC), accounting for 10-15% (~30,000 cases/year in the US) of total breast

114   cancer cases. ILC is defined by the loss of functional E-cadherin *(CDH1),* which occurs in 95%

115   of ILC due to truncating mutations, loss of heterozygosity, and transcriptional repression[23,24].

116   Due to the loss of E-cadherin protein*,* ILC cells grow in linear patterns throughout the breast

117   tissue, lacking the ability to form adherens junctions, in contrast to the solid mass growth of the

118   most frequent subtype of breast cancer, invasive ductal breast carcinoma (IDC)[25]. Interestingly,

119   one of the most IGF1 responsive cell lines in our above-referenced proteomic data set was a

120   human ILC cell line, MDA-MB-134-IV, that lacks E-cadherin protein expression and cell-cell

121   junctions[17]. In this study, we characterize the regulation of IGF1R by E-cadherin, and provide

122   evidence that inhibition of IGF1R in E-cadherin deficient breast cancers could potentially serve

123   as an effective therapeutic strategy.

124

125   **MATERIALS AND METHODS**

126   *Cell culture*

127   Cell lines were authenticated (most recent date listed [ ]) by the University of Arizona Genetics

128   Core and mycoplasma tested (Lonza #LT07-418). Lab stocks were made following

129   authentication and used for this study. MCF-7 (ATCC; DMEM+10% FBS [06/29/16]), T47D

130   (ATCC; RPMI+10% FBS [02/08/17]), ZR75.1 (ATCC; RPMI+10% FBS [10/13/16]), MDA-MB-

131   231 (ATCC; DMEM+10% FBS [10/13/16]), MDA-MB-134-IV (ATCC; 50/50 DMEM/L15+10%

132   FBS [02/08/17]), SUM44PE (Asterand; DMEM/F12+2% CSS with 5ug/ml insulin, 1ug/ml

133   hydrocortisone, 5mM ethanolamine, 5ug/ml transferrin, 10nM triodothyronime, and 50nM

134   sodium selenite [02/08/17 – no reference profile exists in database]), and BCK4[26] (MEM+5%

135   FBS with 1nM insulin and 1x NEAA [10/13/16 – no reference profile exists in database) cells

136   were cultured with indicated media conditions.

137 *Transient siRNA transfection*

138 Cells were reverse transfected with 25nM final concentration of siGENOME human SMARTpool

139 control siRNA (Dharmacon #D-001206) or siGENOME human SMARTpool CDH1 siRNA

140 (Dharmacon #M-003877-02) using Lipofectamine RNAiMAX (Invitrogen #13778) protocol for 48

141 hours. For IGF1 (GroPep BioReagents #CU100) stimulation, cells were serum starved overnight

142 and pulsed with IGF1 (1nM, 10nM, or 100nM) for 10 minutes.

143 *Stable shRNA infection*

144 Stable CDH1 knockdown T47D cells were generated using a retro-viral infection of Renilla

145 control (shSCR [5' TGCTGTTGACAGTGAGCGCAGGAATTATAATGCTTATCTATA

146 GTGAAGCCACAGATGTATAGATAAGCATTATAATTCCTATGCCTACTGCCTCGGA]) and two

147 CDH1 (sh-1 [5' TGCTGTTGACAGTGAGCGCAAGTGTGTTCATTAATGTTTATAGTGAAGCC

148 ACAGATGTATAAACATTAATGAACACACTTATGCCTACTGCCTCGGA] and sh-2 [5' TGCTGT

149 TGACAGTGAGCGACCGGGACAACGTTTATTACTATAGTGAAGCCACAGATGTATAGTAATA

150 AACGTTGTCCCGGGTGCCTACTGCCTCGGA]) short-hairpin RNAs (shRNA). Cells were

151 selected with growth media supplemented with 1ug/ml Puromycin (Life #A11138-03).

152 *Plasmid DNA overexpression*

153 MDA-MB-231 cells were stably transfected using FUGENE6 with empty or hE-cadherin-pcDNA3

154 vector (Addgene #45769) using 15ug DNA per 10cm plate of cells. Cells were selected in

155 growth media supplemented with 800ug/ml G418 (Invitrogen #10131-035).

156 *Immunoblotting*

157 Samples for immunoblot analysis were collected using RIPA buffer (50mM Tris pH 7.4, 150mM

158 NaCl, 1mM EDTA, 0.5% Nonidet P-40, 0.5% NaDeoxycholate, 0.1% SDS, 1x HALT cocktail

159 [Thermo Fisher #78442]) and standard immunoblot technique was followed. Membranes were

160 blocked in Odyssey PBS Blocking Buffer (LiCor #927-40000), and incubated in primary

161 antibodies overnight: pIGF1R Y1135 (Cell Signaling #3918; 1:500), IGF1R β-subunit (Cell

162   Signaling #3027; 1:1000), pAkt S473 (Cell Signaling #4060; 1:1000), total Akt (Cell Signaling

163   #9272; 1:1000), E-cadherin (BD Biosciences #610182; 1:1000), and β-actin (Sigma #A5441;

164   1:5000). Membranes were incubated in LiCor secondary antibodies for 1 hour (anti-rabbit

165   800CW [LiCor #926-32211]; anti-mouse 680LT [LiCor #925-68020]; 1:10,000), and imaged with

166   Odyssey Infrared Imager.

167   *IGF1-induced cell cycle and viability analysis*

168   *For cell cycle*: MCF-7 and ZR75.1 cells were reverse transfected as described above, serum

169   starved for approx. 30 hours, and pulsed with 10nM IGF1 for 17 hours. Cells were fixed in 70%

170   EtOH for 30 minutes at 4˚C and RNA digested using 50ng/ul RNase A (Qiagen #1007885) for

171   15 minutes at 37˚C. DNA content was then stained using 50ng/ul propidium iodide (Sigma

172   #P4170) for 30 minutes at 4˚C. Cell cycle profiles were analyzed using the BD LSRII flow

173   cytometer and analyzed using the FACS DIVA software. The statistical difference in percent of

174   cells in S- or G2/M phase in IGF1 treated cells over vehicle control in experimental groups was

175   evaluated using a two-tailed student's t-test (p<0.05).

176   *For viability*: T47D shSCR and shCDH1 #1 and #2 cells were plated in serum-free media in 96

177   well plates (9,000 cells/well) and then stimulated with IGF1 (10nM) for 6 days. The FluoReporter

178   Blue Fluorometric dsDNA Quantitation Kit was used to measure DNA content. Statistical

179   difference in Hoechst fluorescence in IGF1 treated cells over vehicle control in each cell line

180   was evaluated using a two-tailed student's t-test (p<0.05).

181   *Immunofluorescence and Proximity ligation assay (PLA)*

182   Cells were plated on coverslips and fixed in 4% paraformaldehyde for 30 minutes at 37˚C.

183   Coverslips were permeabilized for 1 hour using PBS+0.3% Triton X-100. For

184   immunofluorescence, coverslips were blocked in PBS+5% goat serum, incubated in primary

185   antibody overnight (total IGF1R β-subunit [Cell Signaling #3027; 1:300] and E-cadherin [BD

186   Biosciences #610182; 1:100]), followed by Alexa Fluor secondary antibody incubation for 1 hour

187   (anti-rabbit Alexa Fluor 488 [Life Technologies #A11070] and anti-mouse Alexa Fluor 546 [Life

188   Technologies #A11018]; 1:200). For *in situ* proximity ligation assay, coverslips were processed

189   using the Duolink Red mouse/rabbit kit using the protocol provided (Sigma #DUO92101) with

190   the antibody dilutions above. The ratio of puncta/nuclei for each experimental condition was

191   calculated by counting all puncta and nuclei in five 60x images. One-way ANOVA was used to

192   compare the ratios between the experimental conditions (VHC, 30m, 6hr, 24hr). Confocal

193   microscopy was used for imaging.

194   *Dose response growth assays and synergy measurements*

195   MCF-7 and ZR75.1 cells were reverse transfected with control or CDH1 siRNA as described

196   above into 96-well plates (9,000 cells/well) in 100ul of media/well. Cells were treated with 3x

197   vehicle (DMSO), OSI-906 (Selleckchem #S1091) or BMS-754807 diluted in 50ul of media for a

198   final volume in each well of 150ul (n=6 per concentration). Plates (2D and ultra-low attachment

199   [ULA; Corning #3474]) were collected on day 6 and viability was measured using CellTiter Glo

200   Viability assay (Promega #G7572). EC_{50} values for viability were calculated by non-linear

201   regression and statistical differences evaluated using sum-of-squares Global f-test ($p<0.05$). For

202   synergy experiments, SUM44PE and MDA-MB-134 cells were plated in 96-well ULA plates

203   (18,000 cells/well) in 100ul of media/well. Cells were treated with 6x vehicle (DMSO), OSI-906,

204   BMS-754807, or BEZ235 (Selleckchem #S1009) diluted in 25ul of media such that the

205   combination of two drugs resulted in 150ul of total volume in each well (n=2 per experiment).

206   Synergy was calculated using the Median-Effect Principle and Combination Index-Isobologram

207   Theorem (Chou-Talalay)[27]. Combination index values for ED50, ED75, ED90 are shown as a

208   mean ± SEM from n=3 independent experiments.

209   *In vivo ILC xenograft growth and explant culturing*

210   MDA-MB-134 cells ($5x10^6$ cells) and BCK4 cells ($5x10^6$ cells) were injected into the right

211   inguinal mammary fat pads of 7-8 week old NOD.Cg-Prkdcscid Il2rgtm1Wjl/SzJ (NSG; The

212   Jackson Laboratory) and NOD.CB17-Prdkcscid/J mice (NOD SCID; The Jackson Laboratory),

213   respectively (implanted with 0.36mg 90-day slow release estradiol pellets [Innovative Research

214   of America #SE-121]) and grown to a tumor volume of 350mm^3. Tumors were collected, minced

215   into 1-2mm^3 chunks of tumor tissue, and plated onto Vetspon Absorbable Hemostatic Gelatin

216   sponges (Patterson Veterinary #07-849-4032) in 12-well tissue culture plates containing 1.5mls

217   of explant media (DMEM/F12+10% FBS with 10mM HEPES, 1mg/ml BSA, 10ug/ml insulin,

218   10ug/ml hydrocortisone, 1x antibiotic-antimycotic solution [Thermo Fisher #15240-062]). Media

219   was treated with vehicle or 1uM BMS-754807 for 72 hours. Tissue was collected by formalin

220   fixation followed by paraffin embedding. Sections were stained for Ki67 (Dako #M7240; 1:100)

221   using standard immunohistochemistry technique. Nuclei were quantified by counting all clearly

222   defined nuclei within each tissue section (n=3-6). Two-tailed student's t-test was used to

223   determine statistical difference between vehicle and BMS-754807 treatment (p<0.05).

224   *TCGA Data Analysis*

225   TCGA RNA-seq expression data were downloaded as transcripts per million (TPM) from the

226   Gene Expression Omnibus database (GEO: GSE62944) and log2(TPM+1) for gene-level

227   results were used. TCGA Reverse Phase Protein Array (RPPA) data were downloaded as

228   median-normalized, batch-corrected expression values from TCPA (Level 4, version 4.0). ER+

229   IDC (n=417) and ILC (n=137) samples with both RNA-Seq and RPPA data were used for all

230   analyses. Mann-Whitney U tests were used to compare expression, Spearman's rho to compare

231   correlations, and a chi-square test to compare proportions between ILC and IDC tumors. All

232   were calculated using R (version 3.4.1). The median expression values for IGF1 and pIGF1R

233   across ER+ IDC and ILC tumors (n=554) were used as cutoffs for Figure 4G.

234

235

236

237   **RESULTS**

238   _Loss or inhibition of E-cadherin results in enhanced IGF1R activity_

239   To validate our previously published data[17] and to further understand the regulation of the IGF1

240   signaling pathway by E-cadherin, we silenced E-cadherin (_CDH1_) by siRNA knockdown in a

241   panel of three estrogen receptor (ER)-positive IDC cell lines and then stimulated with a dose

242   series of IGF1 (0, 1, 10, 100nM). MCF-7, ZR75.1, and T47D E-cadherin knockdown (siCDH1)

243   cells showed enhanced sensitivity to IGF1 compared to the scramble control (siSCR) cells, most

244   notable at the 1nM dose of IGF1, resulting in increased phosphorylation of IGF1R and Akt (Fig

245   1A-C). As a complementary approach, we inhibited E-cadherin function in MCF-7 cells using the

246   HECD-1 monoclonal antibody that binds the extracellular domain of E-cadherin and prevents

247   adherens junction formation. Similar to the knockdown of E-cadherin, HECD-1 treated cells

248   showed increased IGF1R and Akt phosphorylation compared to control (Fig 1D). Additionally,

249   we evaluated confluency-dependent IGF1R signaling to understand the effect of increased cell-

250   cell contacts. A confluent monolayer of MCF-7 cells lost the ability to initiate IGF1R signaling

251   upon ligand stimulation compared to a sub-confluent monolayer (approx. 40-50%), however, the

252   knockdown of E-cadherin rescued signaling in both confluency conditions (Fig 1E).

253   We evaluated the functional effect of enhanced IGF1 signaling on the cell cycle profile in MCF-7

254   and ZR75.1 cells with reduced E-cadherin. CDH1 knockdown cells showed a significant

255   increase (p=0.03 and p=0.0005, respectively) in the percentage of cells progressing into the S-

256   and G2/M-phases of the cell cycle following IGF1 treatment compared to siSCR cells (Fig 1F).

257   Similarly, slight increases in IGF1-induced cell viability in siCDH1 compared to siSCR in T47D

258   cells were observed (Fig S1).

259   We overexpressed E-cadherin in MDA-MB-231 cells, an ER-negative IDC cell line with

260   undetectable E-cadherin protein by immunoblot to determine if overexpression represses

261   signaling. Although adherens junction formation was not observed (data not shown), E-cadherin

262   overexpressing cells demonstrated decreased phosphorylation of IGF1R and Akt compared to

263   empty vector control cells, and significantly less cell cycle progression in response to IGF1

264   stimulation (p=0.011; Fig S2).

265   *Loss of E-cadherin enhances sensitivity to IGF1R inhibition*

266   Due to the enhanced sensitivity of E-cadherin knockdown cells to IGF1 stimulation, we

267   determined if loss of E-cadherin in MCF-7 and ZR75.1 cells also increased sensitivity to the

268   IGF1R ATP-competitive small molecule inhibitors, OSI-906 (OSI) and BMS-754807 (BMS). In

269   addition to 2D adherent culture, ultra-low attachment suspension growth (ULA) was examined,

270   since we observed increased cell viability in E-cadherin knockdown cells under these conditions

271   (Tasdemir et al, manuscript in preparation), possibly due to the reported annoikis resistance of

272   cells lacking E-cadherin expression[28]. MCF-7 siCDH1 cells displayed significantly decreased

273   viability in response to OSI treatment, compared to siSCR cells in both 2D (p<0.0001; Fig 2A)

274   and ULA (p=0.0003; Fig 2B) growth conditions resulting in a shift in the EC_{50}. Additionally,

275   ZR75.1 siCDH1 cells showed significantly decreased viability and a shift in the EC_{50} when

276   grown in ULA (p<0.0001; Fig S3) in response to OSI treatment, but not in the 2D growth

277   condition. Similarly, MCF-7 siCDH1 cells showed decreased viability in response to BMS

278   compared to siSCR cells the ULA growth condition (p<0.0001), but no significant difference in

279   2D (Fig 2C-D). Overall, these data suggest that the loss of E-cadherin enhances breast cancer

280   cell sensitivity to IGF1R inhibition. We also tested the growth response of MCF-7 siSCR and

281   siCDH1 cells treated with ICI 182,780 (ICI), a selective estrogen receptor downregulator

282   (SERD), and observed no statistical difference in EC_{50} suggesting that the loss of E-cadherin

283   does not generally sensitize cells to all small molecule drug treatments (Fig S4).

284

285

286   *IGF1R and E-cadherin directly interact in ER+ breast cancer cells resulting in recruitment of*

287   *IGF1R to adherens junctions*

288   To understand how E-cadherin regulates IGF1R, we assessed whether IGF1R and E-cadherin

289   directly interact in breast cancer cells using *in situ* proximity ligation assay (PLA). The sensitivity

290   and specificity of PLA allows for detection of endogenous interacting proteins within proximity of

291   no further than 40nm. PLA showed that IGF1R and E-cadherin directly interact in both MCF-7

292   and T47D cells, as shown by the red fluorescent puncta (Fig 3A-B). To demonstrate the

293   specificity of the detection, we used MCF-7 knockdown cells lacking E-cadherin (siCDH1) or

294   IGF1R (siIGFR) as negative controls and observed the red fluorescent puncta signal greatly

295   diminished (Fig 3C-D, Fig S5A-C). Additionally, secondary antibody specificity was confirmed by

296   using each primary antibody alone and a no primary antibody control and did not detect

297   significant levels of PLA puncta over background (Fig S5D-F). The interaction between IGF1R

298   and E-cadherin following IGF1 stimulation was examined using PLA. In MCF-7 cells, IGF1

299   treatment caused a significant decrease in number of fluorescent puncta (p=0.003), suggesting

300   that the interaction between the two proteins needs to be disrupted for proper IGF1R function

301   (Fig 3E-I), possibly explaining why siCDH1 cells have an increased IGF1R signaling capacity

302   compared to control cells.

303   We stained MCF-7 cells for endogenous IGF1R and E-cadherin and determined that IGF1R and

304   E-cadherin co-localize to adherens junctions. Interestingly, co-localization was prominent at the

305   points of cell-cell contact, and noticeably absent or reduced on portions of the membrane where

306   there was no cell-cell contact (Fig 3J). This suggests that E-cadherin recruits IGF1R to

307   adherens junctions, perhaps to sequester the receptor as a mechanism of signaling repression.

308   Upon knockdown of E-cadherin the expression pattern of IGF1R appears to redistribute equally

309   to the entire cell membrane (Fig 3K) supporting the idea that E-cadherin influences and

310   regulates IGF1R localization.

311 *Invasive lobular breast cancers (ILC) display enhanced IGF1-IGF1R pathway activation*

312 Because knockdown or inhibition of E-cadherin induces hyperactivity of the IGF1R pathway in

313 cell line models, we investigated whether IGF1R pathway activity is also hyperactivated in ILC,

314 a subtype of breast cancer that accounts for 10-15% of all breast cancer cases and is

315 molecularly classified by its genetic loss of E-cadherin[23]. Because 90-95% of ILC tumors are

316 ER+, we focused on this cohort[23]. IGF1R expression and localization was examined in the ER+

317 ILC cell lines: MDA-MB-134 (MM134; Fig 4A), SUM44PE (Fig 4B), and BCK4 (Fig 4C). IGF1R

318 staining was membranous similar to that observed in MCF-7 siCDH1 cells (Fig 3F). As

319 expected, ILC cells showed a lack of membranous E-cadherin staining (Fig 4A-C).

320 To compare IGF1R activity in ER+ ILC and IDC tumors, CDH1 and IGF1 ligand mRNA

321 expression, and IGF1R phosphorylation (pIGF1R; Y1135/Y1136) were examined using RNA-

322 sequencing and Reverse Phase Protein Array data from The Cancer Genome Atlas (TCGA).

323 Concurrent with a decrease in CDH1 mRNA expression (p=9.06e-52; Fig 4D), IGF1 ligand

324 mRNA expression (p=1.3e-15; Fig 4E) and pIGF1R levels (p=2.15e-08; Fig 4F) were

325 significantly increased in the ILC tumors compared to IDC tumors. Interestingly, ILC tumors

326 exhibited a significant positive correlation between IGF1 mRNA expression and pIGF1R level

327 (Spearman rho=0.21; p=0.012), despite having significantly reduced total IGF1R expression

328 compared to IDC (data not shown; Fig 4G). In contrast, IDC tumors did not show a correlation

329 (Spearman rho=0.06; p=0.22) suggesting that presence of IGF1 ligand did not necessarily

330 activate IGF1R in IDC. Strikingly, the percentage of tumors with higher than median expression

331 (across all breast tumors) of both IGF1 and pIGF1R is significantly higher in ILC (56.2%)

332 compared to IDC (21.3%), suggesting that IGF1 ligand activates IGF1R signaling in these

333 tumors more efficiently with the loss of E-cadherin (chi-square test, p= 2.5e-14 [Fig 4G]).

334 Interestingly, when assessing activation of the IGF-sig[16] in ER+ ILC versus IDC in the TCGA

335 cohort we did not observe a difference in expression score (data not shown).

336   *IGF1R inhibitors and endocrine therapy synergize to decrease viability in ILC cells*

337   Clinically, patients with ER+ ILC are treated with endocrine therapy targeting ER, however, data

338   from the BIG 1-98 trial suggest that ILC tumors demonstrate resistance to tamoxifen, a selective

339   estrogen receptor modulator, compared to IDC[29]. Additionally, results from multiple clinical

340   studies indicate that ILC patients have a poorer prognosis with more frequent late recurrences

341   compared to IDC[30–32]. This highlights the need to improve therapeutic options in ILC patients

342   based on uniquely activated pathways and therefore, we evaluated efficacy of IGF1R pathway

343   inhibitors in ER+ ILC cell lines in combination with endocrine therapy. Recent data published

344   from our lab suggest that tamoxifen, can act as a partial ER agonist activating ER activity in

345   some ILC cell lines, rather than a pure antagonist as in IDC cells[33], in line with the data from the

346   BIG1-98 study. Therefore, we tested efficacy of the selective estrogen receptor downregulator,

347   ICI 182,780 (ICI) in combination with two IGF1R inhibitors used in Figure 2 (OSI and BMS) and

348   a PI3K/mTOR inhibitor (BEZ235 [BEZ]). SUM44PE and MM134 cells were treated with

349   increasing doses of OSI (Fig 5A-B; Fig S6A-B), BMS (Fig 5C-D; Fig S6C-D), and BEZ (Fig 5E-

350   F; Fig S6E-F) in combination with increasing doses of ICI. With all three IGF1R pathway

351   inhibitors, decreased cell viability was observed with the addition of increasing doses of ICI.

352   Formal synergy testing of the drug combinations using the Median-Effect Principle and

353   Combination-Index Isobologram Theorem, commonly referred to as the Chou-Talalay method[27]

354   revealed combination index (CI) values less than 1 for drug interactions at the ED50, ED75, and

355   ED90 indicating a high level of synergy for the three sets of inhibitor combinations (Fig 5, Fig

356   S6, Table S1). The lowest CI values were observed for the BMS+ICI drug combination in

357   SUM44PE cells (ED50=0.127, ED75=0.081, ED90=0.099). Additionally, a minimum dose

358   reduction index (DRI) for ICI of 8-fold for all drug combinations in SUM44PE cells and 2-fold in

359   MM134 cells at the EC50 was seen. This data suggests that adding an IGF1R pathway inhibitor

360   in combination with ICI reduces the concentration of ICI necessary to achieve that same

361   inhibitory effect as ICI alone.

362   *Ex vivo IGF1R inhibition inhibits proliferation in an ILC xenograft*

363   Finally, we evaluated the efficacy of an IGF1R inhibitor in ILC tumors. However, there are a

364   limited number of ILC patient-derived xenograft (PDX) and cell line xenograft models, and their

365   slow growth rates makes large scale *in vivo* studies challenging. We therefore treated two ILC

366   cell line xenografts *ex vivo* as explant cultures, as previously described[34–37]. The advantages of

367   this technique include less tissue requirement for the assay compared to an *in vivo* study and

368   rapid understanding of the therapeutic efficacy of the inhibitor. Additionally, data published by

369   Majumder et al.[37] suggest a high concordance between *ex vivo* and *in vivo* tumor response to

370   drug treatment. MM134 and BCK4 cells (a weakly ER responsive ILC cell line, not used for

371   synergy experiments due to slow growth *in vitro*) were grown as xenografts, harvested and

372   plated as explant culture, and treated with vehicle or BMS (1µM) for 72 hours. The tissue was

373   collected and stained for Ki67 as a marker of proliferation. We observed a significant decrease

374   in Ki67 positive nuclei in both tumor models treated with BMS (Fig 6). In the MM134 tumor we

375   observed a significant decrease (p=0.002) in Ki67 positive nuclei from 47% in the vehicle to

376   22% in the BMS treated tumor tissue (n=3 or 4; Fig 6A-C). Similarly, in the BCK4 tumor we

377   observed a significant decrease (p=0.005) in Ki67 positive nuclei from 25% in the vehicle to

378   11% in the BMS treated tumor tissue (n=6; Fig 6D-F). This data suggest that targeting IGF1R in

379   ILC tumors may be a useful strategy to inhibit cell proliferation.

380

381   **DISCUSSION**

382   Despite a large body of preclinical evidence supporting the use of IGF1R inhibitors for the

383   treatment of breast cancer, the outcomes of clinical trials testing the efficacy of these drugs in

384   patients thus far have been disappointing. However, these trials proceeded with a lack of

385   appropriate biomarkers for predicting positive therapeutic efficacy and little to no understanding

386   of which tumor types would benefit[13–15,38]. In response, in recent years the field has emphasized

387   the need to understand and identify gene expression or proteomic biomarkers that predict a

388   positive response to targeted therapy. Along this thought process, we previously published a

389   gene expression signature used to identify tumors that are IGF1 responsive[16] and here we focus

390   on one proteomic biomarker, E-cadherin, identified through an integrative computational

391   approach recently published by our group[17]. It is known that constitutive IGF1R activation drives

392   E-cadherin transcriptional repression through EMT[6,10], however, the reverse regulation of IGF1R

393   by E-cadherin has not been previously characterized. Our data suggest that loss of E-cadherin

394   in breast tumors, specifically in ILC, highlights a subset of tumors that may be responsive to

395   IGF1R inhibition and here we begin to describe the mechanism by which this regulation occurs.

396   We demonstrate that in breast cancer cells, IGF1R is endogenously localized to cell-cell

397   contacts, similar to data published in MCF-7 cells overexpressing IGF1R[39] and in corneal

398   epithelial cells[40]. We show a direct, endogenous interaction between IGF1R and E-cadherin

399   using *in situ* proximity ligation assay. To our knowledge interaction between IGF1R and E-

400   cadherin in breast cancer cells has only been demonstrated by immunoprecipitation (IP)[39]. Our

401   data provide confirmation of this interaction using a technique known to be higher in specificity

402   and sensitivity compared to IP, which requires intense cell manipulation (e.g. lysis and scraping)

403   and often results in pull-down of entire protein complexes. This suggests that IGF1R is recruited

404   to adherens junctions by E-cadherin, possibly resulting in receptor sequestration and signaling

405   repression. This process is similar to the sequestration of EGFR into the adherens junction and

406   loss of receptor mobility, a well characterized mechanism of EGFR signaling repression[41–43].

407   However, data published by Curto et al. suggests that the latter action is mediated through the

408   tumor suppressor, Merlin, responsible for coordinating stabilization of the adherens junction and

409   thereby regulating contact-inhibition growth[43]. Although IGF1R signaling is controlled in a

410   contact-dependent manner (Fig 1E), they also showed that IGF1 activity is not regulated by

411   Merlin, indicating that IGF1R regulation by E-cadherin likely occurs independent of this factor[43].

412   Although there may be a yet undefined intermediate regulator similar to Merlin, our data indicate

413   that E-cadherin plays a role in coordinating the recruitment and sequestration of IGF1R within

414   the adherens junction to repress IGF1R signaling. When E-cadherin is lost and junction

415   formation is disrupted (such as in ILC cells), IGF1R is released and re-localizes to the entirety of

416   the cell membrane where signaling is more easily initiated upon IGF1 ligand binding.

417   Supporting this concept, our data indicate that the knockdown of E-cadherin in three ER+ breast

418   cancer cell lines not only enhanced IGF1-induced signaling via IGF1R but also increased

419   sensitivity of the cells to the ligand. This is similar to the relationship reported between EGF-

420   EGFR and IGF1-IGF1R upon adherens junction disruption via calcium-depletion[41]. Because of

421   the increased IGF1R pathway activation associated with the loss of E-cadherin, the knockdown

422   cells in turn became more sensitive to IGF1R inhibition.

423   We believe that IGF1R signaling may be particularly important in ILC, an understudied subtype

424   of breast cancer, due to the complete loss of E-cadherin protein and/or adherens junction

425   formation. In this subtype, the loss of E-cadherin may serve as a biomarker of IGF1 activity.

426   Indeed, we demonstrate that ILC have increased IGF1R pathway activation (IGF1 ligand

427   expression and pIGF1R levels) compared with IDC. This is similar to the results of two studies

428   analyzing differences between ILC and IDC that found increased IGF1 ligand and IGF1R

429   expression levels in ILC[44,45]. Consistent with this, we found that ILC cell lines are susceptible to

430   IGF1R inhibition and importantly, that IGF1R pathway inhibitors (OSI, BMS, BEZ) synergize with

431   a standard of care endocrine therapy (ICI) resulting in further reduced cell growth. Future

432   studies will focus on validating these therapies in additional ILC tumors and understanding the

433   synergistic interaction between IGF1R inhibitors and ICI. This data may be especially important

434   given that there is an increased prevalence of late recurrences in ER+ ILC compared to ER+

435   IDC tumors treated with endocrine therapy, indicating the need for improved therapy options for

436   patients with ILC[29,30].

437   One limitation for the use of IGF1R inhibitors in ILC is the relatively high prevalence of

438   mutations in the PI3K/Akt signaling pathway. Recently, Ciriello et al. comprehensively

439   characterized ILC tumors compared to IDC tumors and described the mutational landscape of

440   127 ILC tumors[23]. They found that 48% of ILC harbor hotspot/missense mutations in *PIK3CA*

441   and 13% have alterations in *PTEN*, similar to previously published data[25,45]. These genetic

442   alterations likely lead to the elevated Akt signature they reported in these tumors. Our data

443   suggest that the remaining tumors may also have high PI3K/Akt signaling activity due to

444   aberrant IGF1R activity. But, because the alterations in *PIK3CA/PTEN* occur downstream of

445   IGF1R, the effectiveness of IGF1R inhibition in this setting is unclear. Resistance to other

446   upstream kinase inhibitors in tumors harboring activating alterations in *PIK3CA/PTEN* has been

447   previously observed[47] and therefore, it would be important to screen patients for these

448   alterations before considering use of receptor tyrosine kinase inhibitor therapy. However, the

449   use of a PI3K pathway inhibitor, such as BEZ235, may be mutually beneficial in targeting the

450   *PIK3CA/PTEN* alterations and the enhanced IGF1R pathway activation observed in these

451   tumors. Interestingly, Cantley et al. recently reported that high levels of insulin promote

452   resistance to PI3K inhibitors in tumors with *PIK3CA* mutations[48], and therefore there may also

453   be a role for combinatorial IGF1R and PI3K inhibition. Future studies are warranted to

454   investigate these relationships using additional *ex vivo* or *in vivo* screening of ILC tumors.

455   In summary, we present a diverse set of data indicating that the loss of E-cadherin enhances

456   IGF1R pathway activity and sensitivity to IGF1R therapy, specifically in ILC. We show that

457   IGF1R and E-cadherin directly interact, which leads to the sequestration and potential

458   repression of IGF1R within the adherens junction. Overall, this study begins to shed light on a

459   previously unrecognized mechanism of IGF1R regulation by E-cadherin and highlights a

460   potential therapeutic strategy of exploiting IGF1R pathway activity in ILC tumors.

461

462   **ACKNOWLEDGEMENTS**

468

469

470

471

472

473

474

475

476

477

478

479

480

481 **REFERENCES**

482 1. Pollak, M. N. Insulin-like growth factors and neoplasia. *Nat. Rev. Cancer* **262,** 84-107-268

483   (2004).

484 2. Becker, M. a, Ibrahim, Y. H., Cui, X., Lee, A. V & Yee, D. The IGF pathway regulates

485   ERα through a S6K1-dependent mechanism in breast cancer cells. *Mol. Endocrinol.* **25,**

486   516–28 (2011).

487 3. Hawsawi, Y., El-Gendy, R., Twelves, C., Speirs, V. & Beattie, J. Insulin-like growth factor

488   - oestradiol crosstalk and mammary gland tumourigenesis. *Biochim. Biophys. Acta* **1836,**

489   345–53 (2013).

490 4. Yee, D. & Lee, A. V. Crosstalk between the insulin-like growth factors and estrogens in

491   breast cancer. *J. Mammary Gland Biol. Neoplasia* **5,** 107–15 (2000).

492 5. Baserga, R., Peruzzi, F. & Reiss, K. The IGF-1 receptor in cancer biology. *Int. J. Cancer*

493   **107,** 873–877 (2003).

494 6. Kim, H.-J. *et al.* Constitutively active type I insulin-like growth factor receptor causes

495   transformation and xenograft growth of immortalized mammary epithelial cells and is

496   accompanied by an epithelial-to-mesenchymal transition mediated by NF-kappaB and

497   snail. *Mol. Cell. Biol.* **27,** 3165–75 (2007).

498 7. Litzenburger, B. C. *et al.* BMS-536924 Reverses IGF-IR-induced Transformation of

499   Mammary Epithelial Cells and Causes Growth Inhibition and Polarization of MCF7 Cells.

500   *Clin Cancer Res* **15,** 1–23 (2009).

501 8. Carboni, J. M. *et al.* Tumor Development by Transgenic Expression of a Constitutively

502   Active Insulin-Like Growth Factor I Receptor. 3781–3788 (2005).

503 9. Sachdev, D., Hartell, J. S., Lee, A. V, Zhang, X. & Yee, D. A Dominant Negative Type I

504 Insulin-like Growth Factor Receptor Inhibits Metastasis of Human Cancer Cells. *J. Biol.*

505 *Chem.* **279,** 5017–5024 (2004).

506 10. Cox, O. T. *et al.* IGF-1 Receptor and Adhesion Signaling: An Important Axis in

507 Determining Cancer Cell Phenotype and Therapy Resistance. *Front. Endocrinol.*

508 *(Lausanne).* **6,** 106 (2015).

509 11. Farabaugh, S. M., Boone, D. N. & Lee, A. V. Role of IGF1R in Breast Cancer Subtypes,

510 Stemness, and Lineage Differentiation. *Front. Endocrinol. (Lausanne).* **6,** 59 (2015).

511 12. Crudden, C., Girnita, A. & Girnita, L. Targeting the IGF-1R: The Tale of the Tortoise and

512 the Hare. *Front. Endocrinol. (Lausanne).* **6,** 64 (2015).

513 13. Boone, D. N. & Lee, A. V. Targeting the Insulin-like Growth Factor Receptor: Developing

514 Biomarkers from Gene Expression Profiling. *Crit Rev Oncog* **17,** 161–173 (2012).

515 14. Singh, P., Alex, J. M. & Bast, F. Insulin receptor (IR) and insulin-like growth factor

516 receptor 1 (IGF-1R) signaling systems: novel treatment strategies for cancer. *Med. Oncol.*

517 **31,** 805 (2014).

518 15. Ekyalongo, R. C. & Yee, D. Revisiting the IGF-1R as a breast cancer target. *npj Precis.*

519 *Oncol.* **1,** 14 (2017).

520 16. Creighton, C. J. *et al.* Insulin-like growth factor-I activates gene transcription programs

521 strongly associated with poor breast cancer prognosis. *J. Clin. Oncol.* **26,** 4078–85

522 (2008).

523 17. Erdem, C. *et al.* Proteomic Screening and Lasso Regression Reveal Differential Signaling

524 in Insulin and Insulin-like Growth Factor I (IGF1) Pathways. *Mol. Cell. Proteomics* **15,**

525 3045–3057 (2016).

526 18. Onder, T. T. *et al.* Loss of E-cadherin promotes metastasis via multiple downstream

527   transcriptional pathways. *Cancer Res.* **68,** 3645–3654 (2008).

528   19.   Hanahan, D. & Weinberg, R. A. Hallmarks of cancer: The next generation. *Cell* **144,** 646–

529   674 (2011).

530   20.   Mauro, L. *et al.* Role of the IGF-I receptor in the regulation of cell-cell adhesion:

531   Implications in cancer development and progression. *J. Cell. Physiol.* **194,** 108–116

532   (2003).

533   21.   Friedl, P. & Alexander, S. Cancer invasion and the microenvironment: Plasticity and

534   reciprocity. *Cell* **147,** 992–1009 (2011).

535   22.   Roxanis, I. Occurrence and significance of epithelial-mesenchymal transition in breast

536   cancer. *J. Clin. Pathol.* **66,** 517–21 (2013).

537   23.   Ciriello, G. *et al.* Comprehensive Molecular Portraits of Invasive Lobular Breast Cancer.

538   *Cell* **163,** 506–519 (2015).

539   24.   Barroso-Sousa, R. & Metzger-Filho, O. Differences between invasive lobular and invasive

540   ductal carcinoma of the breast: results and therapeutic implications. *Ther. Adv. Med.*

541   *Oncol.* **8,** 261–266 (2016).

542   25.   Rakha, E. A. *et al.* Clinical and biological significance of E-cadherin protein expression in

543   invasive lobular carcinoma of the breast. *Am J Surg Pathol* **34,** 1472–1479 (2010).

544   26.   Jambal, P. *et al.* Estrogen switches pure mucinous breast cancer to invasive lobular

545   carcinoma with mucinous features. *Breast Cancer Res. Treat.* **137,** 431–448 (2013).

546   27.   Chou, T. C. & Talalay, P. Quantitative analysis of dose-effect relationships: the combined

547   effects of multiple drugs or enzyme inhibitors. *Adv. Enzyme Regul.* **22,** 27–55 (1984).

548   28.   Derksen, P. W. B. *et al.* Somatic inactivation of E-cadherin and p53 in mice leads to

549   metastatic lobular mammary carcinoma through induction of anoikis resistance and

550   angiogenesis. *Cancer Cell* **10,** 437–449 (2006).

551   29.   Filho, O. M. *et al.* Relative effectiveness of letrozole compared with tamoxifen for patients

552   with lobular carcinoma in the BIG 1-98 Trial. *J. Clin. Oncol.* **33,** 2772–2778 (2015).

553   30.   Pestalozzi, B. C. *et al.* Distinct clinical and prognostic features of infiltrating lobular

554   carcinoma of the breast: Combined results of 15 International Breast Cancer Study Group

555   clinical trials. *J. Clin. Oncol.* **26,** 3006–3014 (2008).

556   31.   Chen, Z. *et al.* Invasive lobular carcinoma of the breast: A special histological type

557   compared with invasive ductal carcinoma. *PLoS One* **12,** 1–17 (2017).

558   32.   Adachi, Y. *et al.* Comparison of clinical outcomes between luminal invasive ductal

559   carcinoma and luminal invasive lobular carcinoma. *BMC Cancer* **16,** 1–9 (2016).

560   33.   Sikora, M. J. *et al.* Invasive lobular carcinoma cell lines are characterized by unique

561   estrogen-mediated gene expression patterns and altered tamoxifen response. *Cancer*

562   *Res.* **74,** 1463–1474 (2014).

563   34.   Andersen, C. L. *et al.* Active estrogen receptor-alpha signaling in ovarian cancer models

564   and clinical specimens. *Clin. Cancer Res.* clincanres.1501.2016 (2017).

565   doi:10.1158/1078-0432.CCR-16-1501

566   35.   Centenera, M. M., Raj, G. V, Knudsen, K. E., Tilley, W. D. & Butler, L. M. Ex vivo culture

567   of human prostate tissue and drug development. *Nat. Rev. Urol.* **10,** 483–487 (2013).

568   36.   Dean, J. L. *et al.* Therapeutic response to CDK4/6 inhibition in breast cancer defined by

569   ex vivo analyses of human tumors. *Cell Cycle* **11,** 2756–2761 (2012).

570   37.   Majumder, B. *et al.* Predicting clinical response to anticancer drugs using an ex vivo

571   platform that captures tumour heterogeneity. *Nat. Commun.* **6,** 6169 (2015).

572   38.   Gualberto, a & Pollak, M. Emerging role of insulin-like growth factor receptor inhibitors in

573   oncology: early clinical trial results and future directions. *Oncogene* **28,** 3009–3021

574   (2009).

575   39.   Guvakova, M. a & Surmacz, E. Overexpressed IGF-I receptors reduce estrogen growth

576   requirements, enhance survival, and promote E-cadherin-mediated cell-cell adhesion in

577   human breast cancer cells. *Exp. Cell Res.* **231,** 149–62 (1997).

578   40.   Robertson, D. M., Zhu, M. & Wu, Y.-C. Cellular distribution of the IGF-1R in corneal

579   epithelial cells. *Exp. Eye Res.* **94,** 179–86 (2012).

580   41.   Qian, X., Karpova, T., Sheppard, A. M., McNally, J. & Lowy, D. R. E-cadherin-mediated

581   adhesion inhibits ligand-dependent activation of diverse receptor tyrosine kinases. *EMBO*

582   *J.* **23,** 1739–1784 (2004).

583   42.   de-Freitas-Junior, J. C. M. *et al.* Insulin/IGF-I Signaling Pathways Enhances Tumor Cell

584   Invasion through Bisecting GlcNAc N-glycans Modulation. An Interplay with E-Cadherin.

585   *PLoS One* **8,** e81579 (2013).

586   43.   Curto, M., Cole, B. K., Lallemand, D., Liu, C. H. & McClatchey, A. I. Contact-dependent

587   inhibition of EGFR signaling by Nf2/Merlin. *J. Cell Biol.* **177,** 893–903 (2007).

588   44.   Nakagawa, S. *et al.* Tumor microenvironment in invasive lobular carcinoma: possible

589   therapeutic targets. *Breast Cancer Res. Treat.* **155,** 65–75 (2016).

590   45.   Bertucci, F. *et al.* Lobular and ductal carcinomas of the breast have distinct genomic and

591   expression profiles. *Oncogene* **27,** 5359–5372 (2008).

592   46.   Shah, V. *et al.* PIK3CA mutations are common in lobular carcinoma in situ, but are not a

593   biomarker of progression. *Breast Cancer Res.* **19,** 7 (2017).

594   47.   Wang, L. *et al.* PI3K pathway activation results in low efficacy of both trastuzumab and

595   lapatinib. *BMC Cancer* **11,** 11:248 (2011).

596   48.   Lewis Cantley. PI 3-kinase links obesity, insulin resistance, and cancer. in (AACR-NCI-

597   EORTC Molecular Targets and Cancer Therapeutics Meeting, 2017).

598

599

600

601

602

603

604

605

606

607

608

609

610

611

612

613

614

615

616

617 **FIGURE LEGENDS**

618 **Figure 1: Loss or inhibition of E-cadherin (*CDH1*) expression enhances IGF1R signaling.**

619 (A) MCF-7, (B) ZR75.1, and (C) T47D breast cancer cells transfected with SCR (siSCR) or

620 CDH1 (siCDH1) siRNA were stimulated with increasing doses of IGF1 (0-100nM) for 10 min.

621 IGF1R and Akt signaling was assessed by immunoblot. Of note, IGF1R expression could

622 routinely not be detected in ZR75.1. (D) MCF-7 cells were treated with 25ug/ml HECD-1

623 antibody for 24 hours and imaged by phase-contrast microscopy for dissociation of adherens

624 junctions. Cells were stimulated with Vhc or 10nM IGF1 for 10 min and IGF1R and Akt signaling

625 assessed by immunoblot. (E) MCF-7 cells were plated at sub-confluency (200k cells in 6-well)

626 or high confluency (800k cells) and then stimulated with either Vhc or 10nM IGF1 for 10 min.

627 IGF1R signaling was assessed by immunoblot. Representative phase-contrast microscopy

628 images of the cell plating densities are shown. (F) MCF-7 and ZR75.1 siSCR and siCDH1 cells

629 were serum-starved and stimulated with 10nM IGF1 for 17 hours and DNA stained with

630 propidium iodide to measure cell cycle profile. The percent of cells in the IGF1/Vhc conditions in

631 the S- and G2/M phases of the cell cycle for siSCR and siCDH1 are shown (representative

632 experiment shown; n=2 or 3 each with 3 biological replicates).

633

634 **Figure 2: Knockdown of E-cadherin increases sensitivity to IGF1R inhibition in breast**

635 **cancer cells.** MCF-7 cells were reverse transfected with SCR or CDH1 siRNA and seeded into

636 96-well 2D or ULA plates and treated with IGF1R inhibitor (OSI-906 or BMS-754807) for 6 days.

637 Conditions in the panels as follows: (A) OSI-906; 2D, (B) OSI-906; ULA, (C) BMS-754807; 2D,

638 (D) BMS-754807; ULA. The CellTiter Glo assay was used to assess cell viability (relative

639 luminescence). EC50 values for viability were calculated by non-linear regression and statistical

640 differences evaluated using sum-of-squares Global f-test (p<0.05; representative experiment

641 shown; n=3 each with 6 biological replicates).

642 **Figure 3: Proximity ligation assay reveals direct interaction between IGF1R and E-**

643 **cadherin and recruitment of IG1R to adherens junctions.** *In situ* proximity ligation assay

644 (PLA) was used to analyze the direct interaction between IGF1R and E-cadherin in breast

645 cancer cells. (A) MCF-7 and (B) T47D cells were plated on coverslips, fixed, and stained with

646 IGF1R and E-cadherin antibody overnight. The Duolink (Sigma) protocol was followed and

647 coverslips were imaged using confocal microscopy to reveal red puncta. (C) MCF-7 siCDH1 and

648 (D) siIGF1R cells were used as negative controls for the assay to assess primary antibody

649 specificity. MCF-7 cells were plated on coverslips and treated with either (E) Vhc or 10nM IGF1

650 for (F) 30 minutes, (G) 6 hours, or (H) 24 hours. PLA protocol for IGF1R and E-cadherin was

651 followed as described above. (I) Red puncta and nuclei (stained with DAPI) were quantified and

652 displayed as a ratio of puncta/nuclei. All puncta and nuclei in 60x images were counted. One-

653 way ANOVA was used to determine significant difference between groups ($p < 0.05$; one

654 independent experiment, n=5 images per slide counted). The co-localization of IGF1R (green)

655 and E-cadherin (red) was analyzed by immunofluorescence staining in (J) MCF-7 siSCR and

656 (K) siCDH1 knockdown cells.

657

658 **Figure 4: IGF1-IGF1R pathway is active in invasive lobular breast carcinoma with genetic**

659 **loss of *CDH1*.** (A) SUM44PE, (B) MDA-MB-134, and (C) BCK4 ILC cells were immunostained

660 for IGF1R (green) and E-cadherin (red) and imaged by confocal microscopy. Of note, BCK4

661 cells were imaged at an increased exposure compared to MM134 and SUM44PE cells. (D)

662 CDH1 mRNA, (E) IGF1 mRNA, (F) and pIGF1R Y1135 & Y1136 levels in ER+ IDC compared to

663 ER+ ILC in TCGA were plotted using RNAseq (log2 TPM+1) and RPPA (median normalized)

664 data. The TCGA cohort includes n=417 IDC cases and n=137 ILC cases that have matched

665 data for RNAseq and RPPA. Man-Whitney test was used to determine significant differences in

666 expression level between the two subtypes, $p < 0.05$). (G) Correlation between pIGF1R and IGF1

667 ligand expression is plotted for IDC (left) and ILC (right). Spearman's rank correlation was used

668 to demonstrate the correlation between the two variables with significance as defined by

669 p<0.05.

670

671 **Figure 5: IGF1R pathway inhibitors and endocrine therapy synergize to inhibit cell**

672 **viability in ILC breast cancer cells.** SUM44PE ILC cells were plated into 96-well ULA plates

673 and treated for 6 days with increasing doses of (A, B) OSI-906, (C, D) BMS-754807, or (E, F)

674 BEZ235 in combination with increasing doses of ICI 182,780. The dose response curves and

675 heat maps shown indicate inhibition of cell viability (CellTiter Glo). Representative experiment

676 shown; n=3 independent experiments each with 2 biological replicates per combination of

677 doses.

678

679 **Figure 6: IGF1R inhibition reduces Ki67 staining in ILC tumor *ex vivo* culture.** MM134 and

680 BCK4 xenograft tumors were harvested from immunocompromised mice, minced into 1-2mm^3

681 tumor chunks and then plated on gelatin sponges in 12-well plate containing 1.5ml media.

682 Media was treated with DMSO Vhc or 1uM BMS-75807 for 72 hours. Tumor pieces were

683 harvested by FFPE and stained for Ki67 as a marker of proliferation (A-B, MM134; D-E, BCK4).

684 Staining was quantified by counting all clearly defined nuclei in 20x images (C and F). Statistical
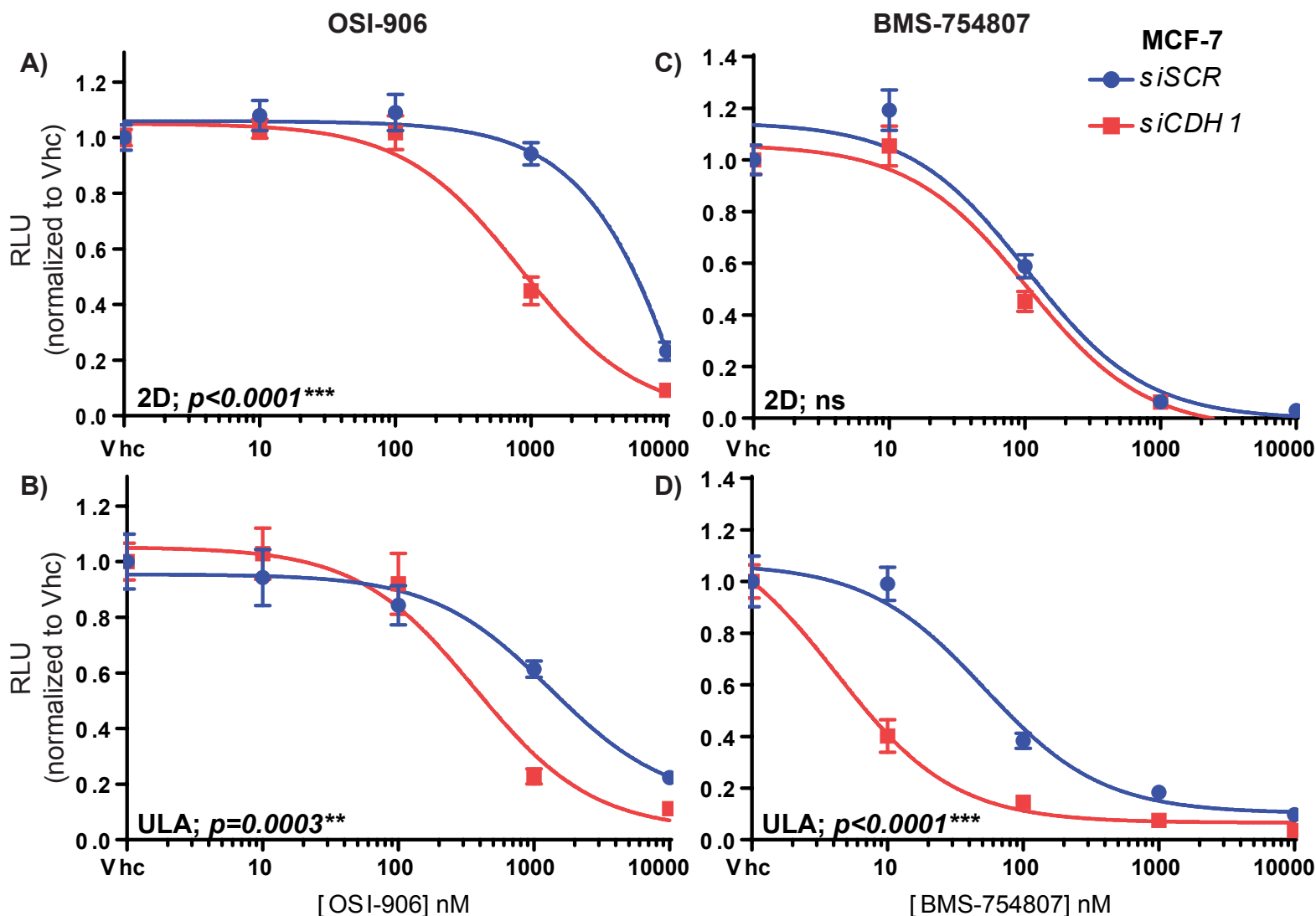
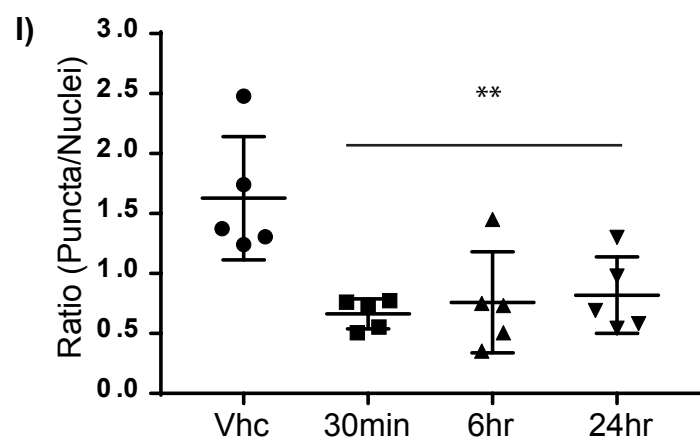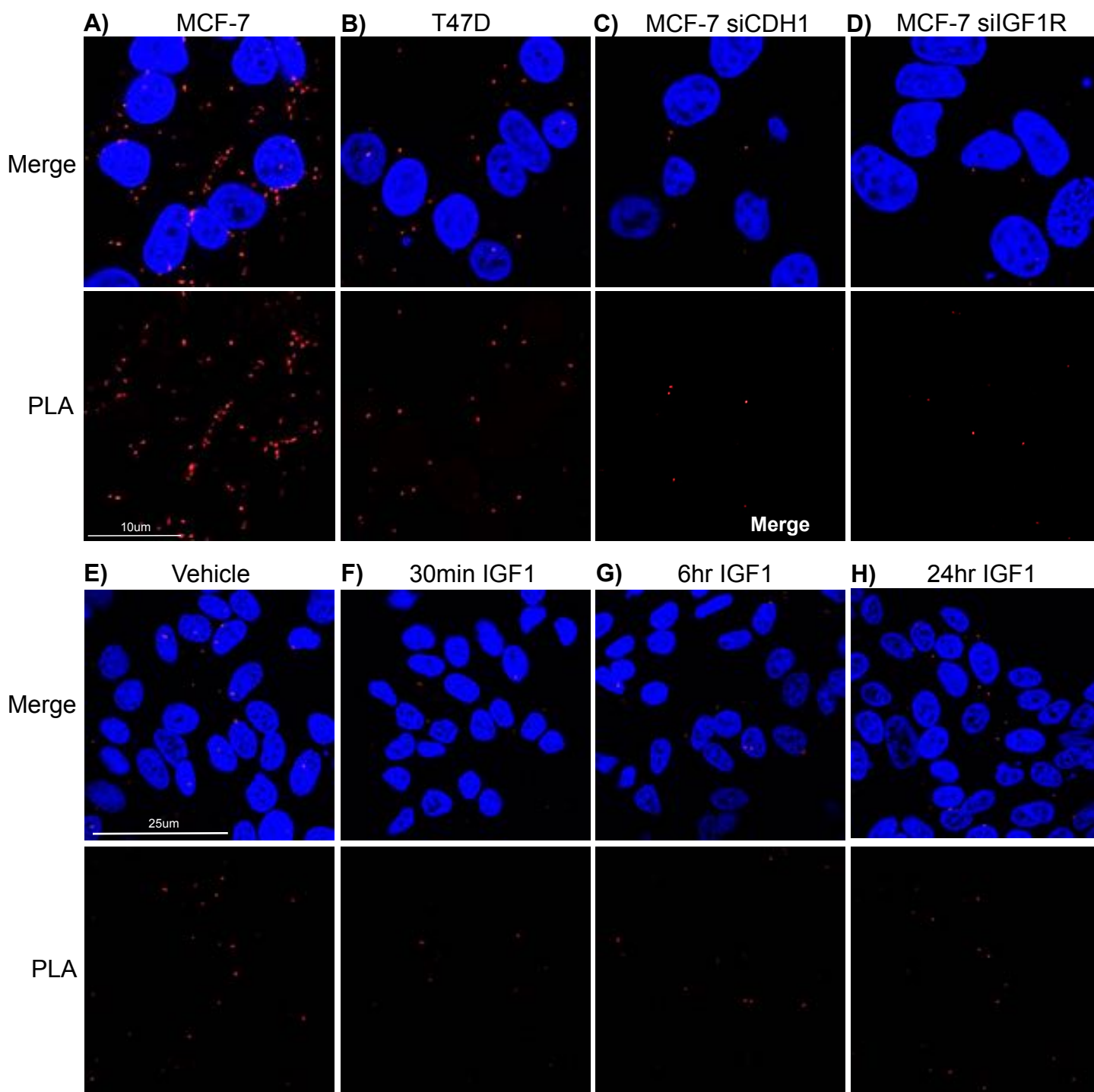685 difference was assessed using a Student's t-test (p<0.05; n=3-6).

686
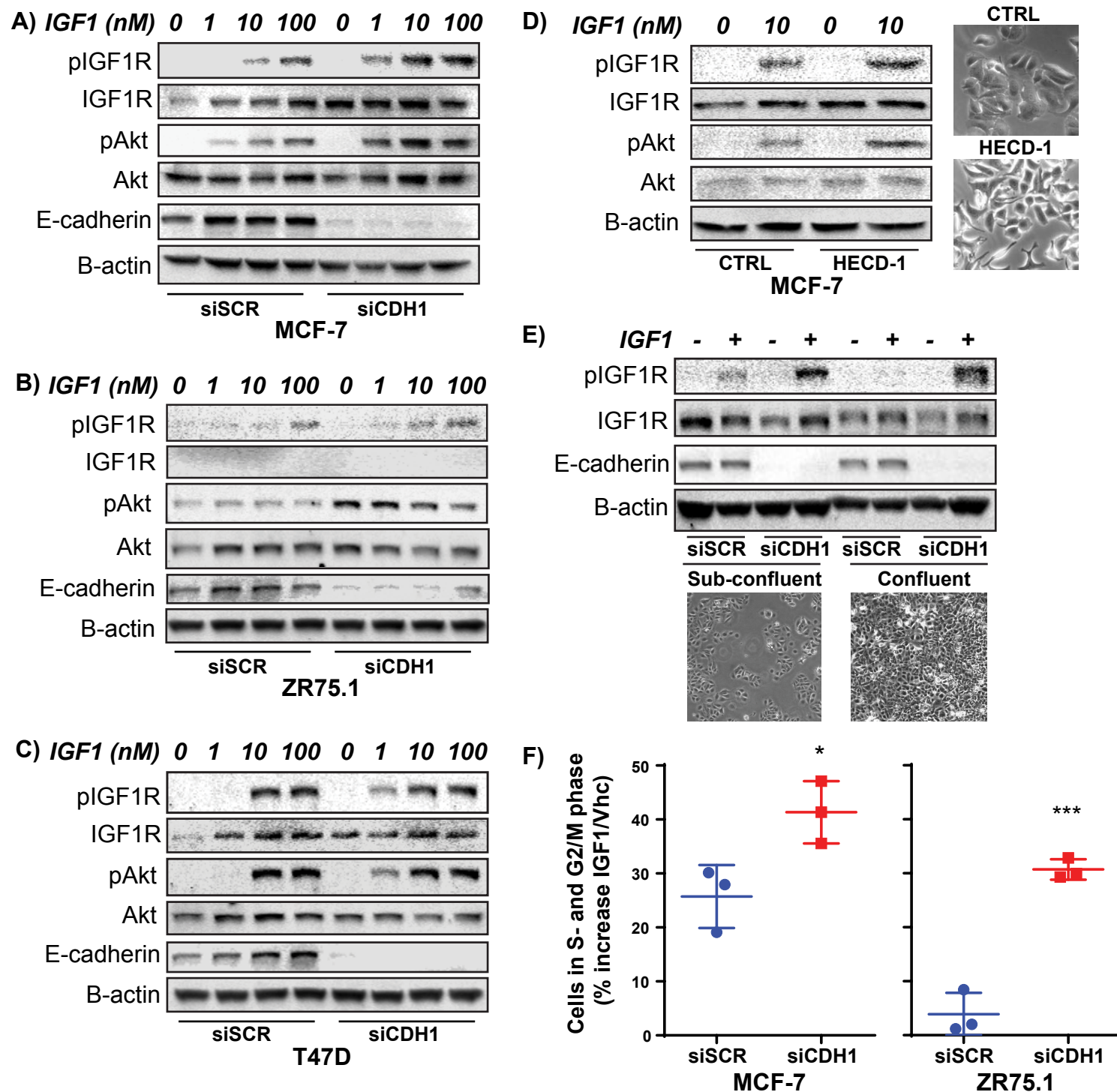
FIGURE 1

FIGURE 2

FIGURE 3 A-I

FIGURE 3 J-K

FIGURE 4

FIGURE 5

FIGURE 6

MM134

BCK4

A)

Vehicle

100 um

D)

Vehicle

100 um

B)

BMS-75807

100 um

E)

BMS-75807

100 um

C)

% Ki67 positive nuclei

**

Vehicle   BMS-75897

F)

% Ki67 positive nuclei

**

Vehicle   BMS-75897